Charged particle's flux measurement from PMMA irradiated by 80 MeV/u carbon ion beam

2012 Phys. Med. Biol. 57 5667

(http://iopscience.iop.org/0031-9155/57/18/5667)

IOP Publishing Physics in Medicine and Biology

Phys. Med. Biol. **57** (2012) 5667–5678 doi:10.1088/0031-9155/57/18/5667

Charged particle's flux measurement from PMMA irradiated by 80 MeV/u carbon ion beam

C Agodi[1], G Battistoni[2], F Bellini[3,4], G A P Cirrone[1], F Collamati[3,4], G Cuttone[1], E De Lucia[5], M De Napoli[1], A Di Domenico[3,4], R Faccini[3,4], F Ferroni[3,4], S Fiore[3], P Gauzzi[3,4], E Iarocci[5,6], M Marafini[3,7], I Mattei[3,4], S Muraro[2], A Paoloni[5], V Patera[5,6], L Piersanti[5,6], F Romano[1], A Sarti[5,6], A Sciubba[5,6], E Vitale[2] and C Voena[3,4]

[1] Laboratori Nazionali del Sud dell'INFN, Catania, Italy
[2] INFN Sezione di Milano, Milano, Italy
[3] Dipartimento di Fisica, Sapienza Università di Roma, Roma, Italy
[4] INFN Sezione di Roma, Roma, Italy
[5] Laboratori Nazionali di Frascati dell'INFN, Frascati, Italy
[6] Dipartimento di Scienze di Base e Applicate per Ingegneria, Sapienza Università di Roma, Roma, Italy
[7] Museo Storico della Fisica e Centro Studi e Ricerche 'E Fermi', Roma, Italy

E-mail: erika.delucia@lnf.infn.it

Received 22 March 2012, in final form 17 July 2012
Published 31 August 2012
Online at stacks.iop.org/PMB/57/5667

Abstract

Hadrontherapy is an emerging technique in cancer therapy that uses beams of charged particles. To meet the improved capability of hadrontherapy in matching the dose release with the cancer position, new dose-monitoring techniques need to be developed and introduced into clinical use. The measurement of the fluxes of the secondary particles produced by the hadron beam is of fundamental importance in the design of any dose-monitoring device and is eagerly needed to tune Monte Carlo simulations. We report the measurements carried out with charged secondary particles produced from the interaction of a 80 MeV/u fully stripped carbon ion beam at the INFN Laboratori Nazionali del Sud, Catania, with a poly-methyl methacrylate target. Charged secondary particles, produced at 90° with respect to the beam axis, have been tracked with a drift chamber, while their energy and time of flight have been measured by means of a LYSO scintillator. Secondary protons have been identified exploiting the energy and time-of-flight information, and their emission region has been reconstructed backtracking from the drift chamber to the target. Moreover, a position scan of the target indicates that the reconstructed emission region follows the movement of the expected Bragg peak position. Exploiting the reconstruction of the emission region, an accuracy on the Bragg peak determination in the submillimeter range has been obtained. The measured differential production rate for protons

produced with $E_{\mathrm{kin}}^{\mathrm{Prod}} > 83$ MeV and emitted at 90° with respect to the beam line is $\mathrm{d}N_{\mathrm{P}}/(\mathrm{d}N_{\mathrm{C}}\mathrm{d}\Omega)\left(E_{\mathrm{kin}}^{\mathrm{Prod}} > 83\ \mathrm{MeV}, \theta = 90^{\circ}\right) = (2.69 \pm 0.08_{\mathrm{stat}} \pm 0.12_{\mathrm{sys}}) \times 10^{-4}\ \mathrm{sr}^{-1}$.

(Some figures may appear in colour only in the online journal)

1. Introduction

Protons and carbon ion beams are presently used to treat many different solid cancers (Jäkel *et al* 2008, Durante and Loeffler 2010) and several new centers based on hadron accelerators are operational or under construction (Amaldi and Kraft 2005, Schardt and Elsässer 2010). The main advantage of this technique, in comparison to the standard radiotherapy with x-ray beams, is the better localization of the irradiation dose in the tumor-affected region sparing healthy tissues and possible surrounding organs at risk. This feature can be achieved because the heavy charged particles loose most of the energy at the end of their range, the Bragg peak (hereafter BP), in comparison to the exponentially decreasing energy release of the x-ray beam. Up to now most of the patients have been treated at centers with proton beams, but routinary use of carbon beams has now started. There are also proposals for future use of ^{4}He, ^{7}Li or ^{16}O beams (Brahme 1986).

New dose-monitoring techniques need to be developed and introduced into clinical use, to meet the improved capability of hadrontherapy to match the dose release with the cancer position. The R&D effort should be then focused to develop novel imaging methods to monitor, preferably in real time, the three-dimensional distribution of the radiation dose effectively delivered during hadrontherapy.

This holds true especially for treatments using carbon ion beams since the dose profile is very sensitive to anatomical changes and minor patients' positioning uncertainties. Conventional methods for the assessment of patients' positioning used in all x-ray-based radiation therapy, where a non-negligible fraction of the treatment beam is transmitted through the patient, cannot be used to pursue this task due to the different physics underlying. All the proposed methods exploit the information provided by the secondary particles produced by the hadron beam along its path to the tumor, inside the patient's body. In particular, it has already been shown that the peak of the dose released by the hadron beam can be correlated with the emission pattern of the flux of secondary particles created by the beam interaction, namely (i) prompt photons within the 1–10 MeV energy range (Stichelbaut and Jongen 2003, Min *et al* 2006, Testa *et al* 2008, 2009) and (ii) pairs of back-to-back photons produced by the annihilation of positrons coming from β^{+} emitters, mainly ^{11}C and ^{15}O (Paans and Schippers 1993, Pawelke *et al* 1997, Parodi *et al* 2002, Enghardt *et al* 2004, Fiedler *et al* 2008, Vecchio *et al* 2009, Attanasi *et al* 2009).

In this paper, we suggest the possibility of correlating the position of the BP in the patient with the emission region of charged secondary particles, mainly protons with kinetic energy $E_{\mathrm{kin}} < 150$ MeV. We report the study of the charged secondary particles produced from the irradiation of a poly-methyl methacrylate (PMMA) with the 80 MeV/u fully stripped carbon ion beam of the INFN Laboratori Nazionali del Sud (LNS). Section 2 is devoted to the description of the experimental setup; the event selection and the spectra of the charged secondary particles are presented in section 3. The analysis of the production region of charged secondary particles is described in section 4, and the measurement of their differential production rate is reported in section 5.

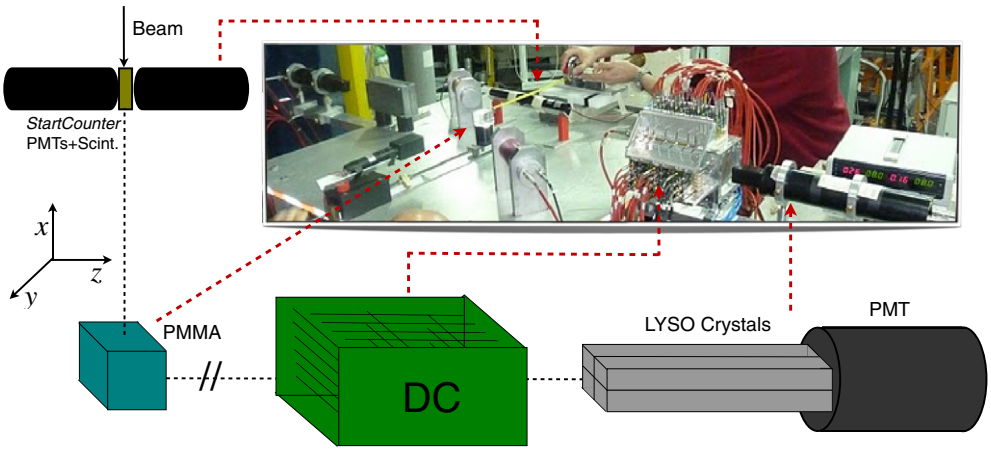

Figure 1. Experimental setup: picture and schematic views. The acquisition is triggered by the coincidence of the start counter and the LYSO detector.

2. Experimental setup

Figure 1 shows the experimental setup. A $4 \times 4 \times 4\,\mathrm{cm}^3$ PMMA target is placed on a 80 MeV/u, fully stripped ^{12}C ion beam. The beam rate, ranging from hundreds of kHz to ∼2 MHz, is monitored with a 1.1 mm thick scintillator placed at 17 cm from the PMMA on the beam line and read out by two photomultiplier tubes (PMTs) Hamamatsu 10583 put in coincidence (start counter). The time structure of the beam has been recorded and monitored feeding the discriminated signals from both the start counter scintillator PMT's in a multi-hit TDC. This setup allowed us to exclude the presence of any beam time structure on a time scale longer than 5 ns.

An array of four LYSO crystals, each measuring $1.5 \times 1.5 \times 12\,\mathrm{cm}^3$, is placed at 90° with respect to the beam line, at 74 cm from the PMMA center. The scintillation light of the crystals is detected with a PMT EMI 9814B triggered in coincidence with the start counter.

A 21 cm long drift chamber (Abou-Haidar *et al* 2012) is placed at 51 cm from the PMMA center, along the flight line connecting the PMMA to the LYSO crystals. We have chosen the configuration at 90° with respect to the beam line to maximize the sensitivity to the BP position along the beam. In the following, the coordinate system is defined (figure 1) with the x-axis along the beam line towards the start counter, the z-axis along the line connecting the centers of PMMA, drift chamber and LYSO crystals detector and the y-axis oriented according to the right-hand rule, and origin at the drift chamber center. The PMMA center in the vertical axis was at $y = -4$ mm. The drift chamber provides a two-dimensional reconstruction of the space point by alternated horizontal (x–z plane V-view) and vertical (y–z plane U-view) layers of wires. Each layer is composed of three $16 \times 10\,\mathrm{mm}^2$ rectangular cells for a total of 36 sense wires (figure 2). The 12 layers, 6 on each view, provide tracking redundancy and ensure high tracking efficiency and excellent spatial resolution. In order to minimize tracking ambiguities, the consecutive layers of each view are staggered by half a cell. Custom front-end electronic boards, designed and realized at the INFN Laboratori Nazionali di Frascati (LNF) electronics workshop, are embedded in the detector and provide single-wire signal amplification by a factor of 10. The drift chamber has been operated with 1.8 kV sense wire voltage, Ar/CO_2 (80/20) gas mixture and 30 mV discriminating threshold for the signals, achieving $\leqslant 200\,\mu$m single-cell spatial resolution and $\simeq 96\%$ single-cell efficiency (Abou-Haidar *et al* 2012). The

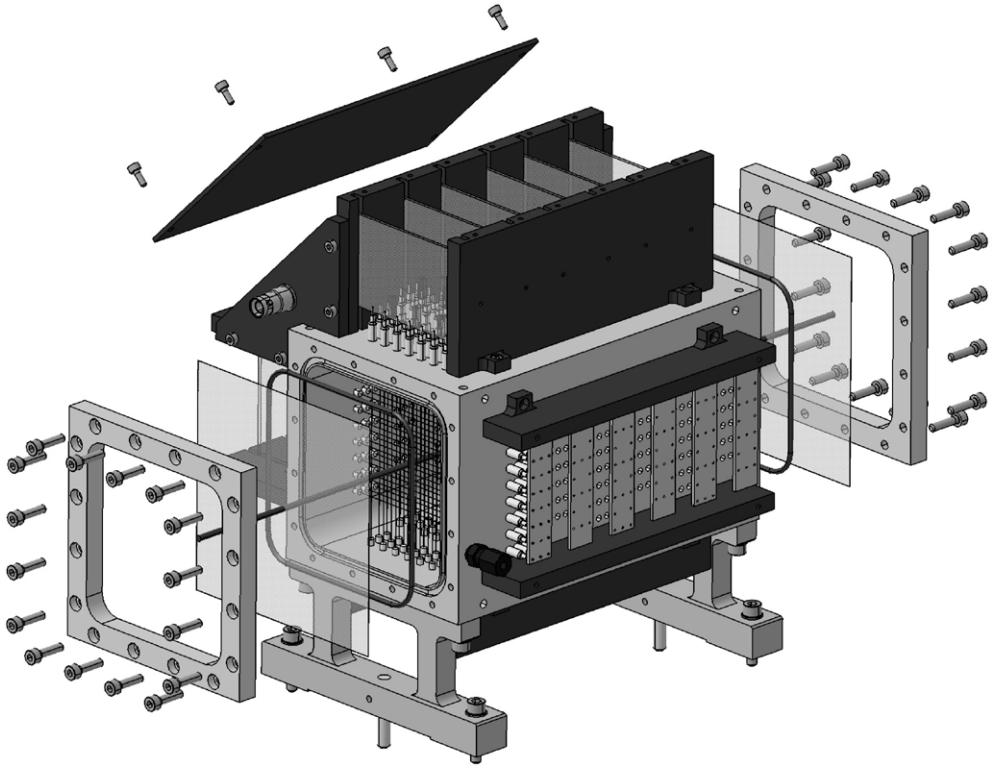

Figure 2. Mechanical drawing of the drift chamber.

signals from the start counter and the LYSO crystals are split and fed into a 12-bit QDC (Caen V792N) and a 19-bit TDC (Caen V1190B), after discrimination, to provide the measurements of both the particles' energy and arrival time. The signals from the 36 cells of the drift chamber are fed, after discrimination, into the same TDC providing the drift time measurements. The front-end electronics has been read out by a VME system using a MOTOROLA 5100 CPU board.

The energy and time calibration of the LYSO crystals and the determination of the drift chamber spacetime relations have been described in Agodi *et al* (2012a, 2012b) and Abou-Haidar *et al* (2012) respectively. A custom tracking algorithm, based on a least-squares iterative fitting method, has been also developed to reconstruct the direction of the charged secondary particles. A first track reconstruction is performed using very clean topologies asking for at least three layers with a single fired cell (hit), on both the V- and U-views. This procedure allows the rejection of hits coming from electronic noise and cross-talk, retaining the information of the physical track. Then a hit addition algorithm improves the tracking performance by using the information from all the other layers.

3. Data selection

The trigger signal is provided by the coincidence of the start counter and LYSO crystals signals, within 80 ns. Figure 3 shows the distribution of the number of hits in the drift chamber (N_{Hits}) obtained for events with detected energy in the LYSO crystals $E_{\mathrm{LYSO}} > 1$ MeV. Events with $N_{\mathrm{Hits}} > 9$ are selected for the analysis of the charged secondary particles.

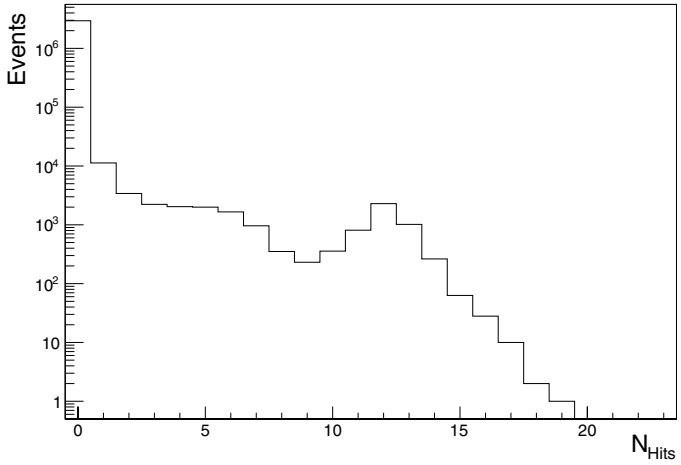

Figure 3. Distribution of the number of fired cells in the drift chamber N_{Hits} for events with detected energy in the LYSO crystals $E_{\mathrm{LYSO}} > 1$ MeV.

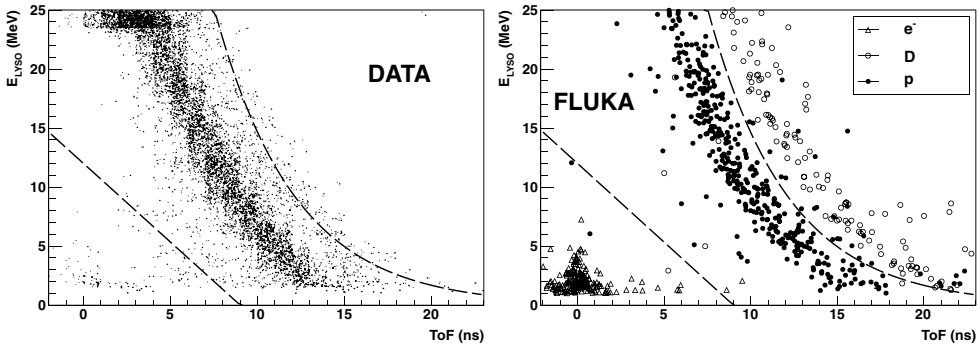

Figure 4. Distribution of the detected energy in the LYSO crystals as a function of the time of flight. Data (left) and FLUKA simulation (right).

In order to evaluate the setup acceptance and efficiency, and to optimize the particle identification analysis a detailed simulation has been developed using the FLUKA software release 2011.2 (Fasso' *et al* 2003, Ferrari *et al* 2005). The detailed geometry description with the setup materials (air included) together with the trigger logic, the time resolution of the scintillator as well as the experimental space resolution of the drift chamber have been considered. The quenching effect in the scintillator has also been introduced in the Monte Carlo according to Koba *et al* (2011). The interaction of a sample of 10^9 carbon ions with 80 MeV/u, equivalent to 10^3 s of data taken at the typical 1 MHz rate of beam, has been simulated. The HADRONTHERAPY default has been used as run condition and the tracking and production of electromagnetic particles below 1 MeV have been avoided to save cpu time. This threshold has been applied after checking that its value has negligible effects on the tracking and energy deposition of the detected secondary protons. To identify the charged particles reconstructed in the drift chamber, we exploit the distribution of the detected energy in the LYSO detector E_{LYSO} as a function of time of flight (ToF), figure 4. In the data sample (left panel) a fast low-energy component due to electrons is clearly visible for ToF values around zero, in the area delimited by the first dashed line. These electrons are produced by

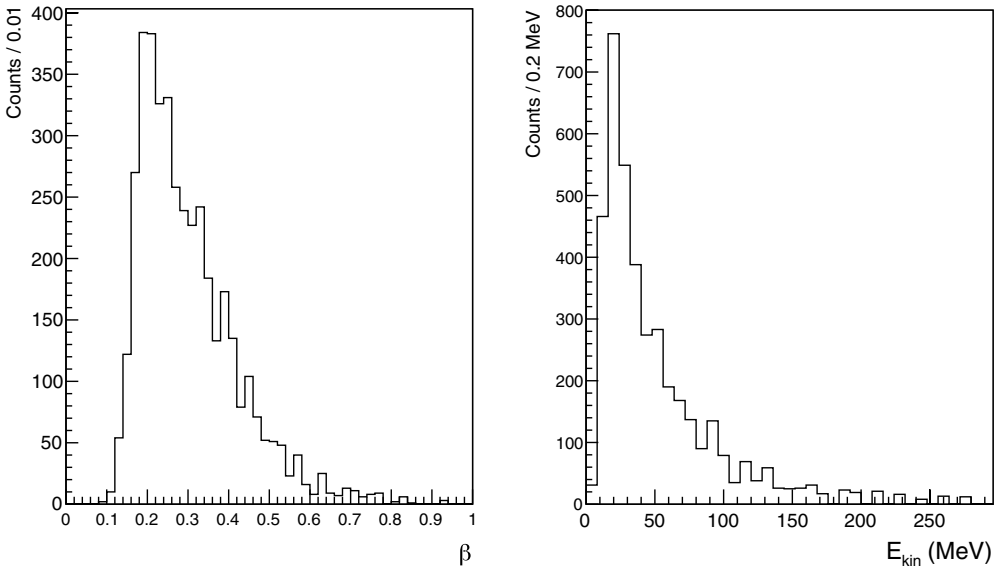

Figure 5 Distribution of $\beta = \frac{v}{c}$ (left) and kinetic energy (right) of charged secondary particles identified as protons.

Compton scattering of the de-excitation photon induced by beam interactions in the PMMA material. The central most populated band, delimited by the two dashed lines, is made by protons with detected energy within a very wide range, originating also the clearly visible saturation of the LYSO crystals QDC for $E_{\mathrm{LYSO}} > 24$ MeV. The FLUKA simulation (right panel) shows similar populations in the (ToF , E_{LYSO}) plane with an additional component of deuterons, above the second dashed line, which is not present in data.

We have then identified as the proton a charged secondary particle with ToF and E_{LYSO} values inside the area delimited by the two dashed lines in figure 4. The systematic uncertainty on the proton/deuteron identification has been estimated using the data events in the deuterons area of the (ToF, E_{LYSO}) plane. Figure 5 shows the distributions of $\beta = \frac{v}{c}$ and the corresponding detected kinetic energy E_{kin} for the identified protons, obtained using the ToF measurement together with the distance between LYSO crystals and PMMA. This detected kinetic energy can be related to the proton kinetic energy at emission time, $E_{\mathrm{kin}}^{\mathrm{Prod}}$, considering the energy loss in the PMMA and the quenching effect of the scintillating light for low-energy protons. The minimum required energy to detect a proton in the LYSO crystals is $E_{\mathrm{kin}}^{\mathrm{Prod}} = 7.0 \pm 0.5$ MeV, evaluated using the FLUKA simulation, and a proton with an average detected kinetic energy $E_{\mathrm{kin}} = 60$ MeV has been emitted with $E_{\mathrm{kin}}^{\mathrm{Prod}} = 83 \pm 5$ MeV. The uncertainty is mainly due to the finite size of both the beam spot $\mathcal{O}(1$ cm) and profile.

In order to use the secondary protons for monitoring purposes, the crossing of some centimeters of patient's tissue has to be considered and therefore the range $E_{\mathrm{kin}} > 60$ MeV of the detected kinetic energy distribution is the most interesting for the above-mentioned application. In the following, the proton kinetic energy detected in the LYSO crystals will be referred to as the kinetic energy.

4. Production region of charged secondary particles

Tracks reconstructed in the drift chamber are backward extrapolated to the PMMA position, to find the production region of charged secondary particles along the path of the carbon ion

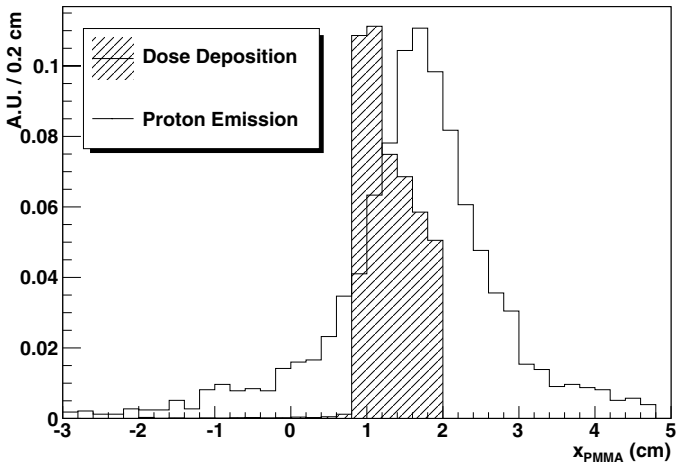

Figure 6. Expected dose deposition in the PMMA evaluated with FLUKA (hatched) compared to the data distribution of x_{PMMA} (solid), the reconstructed emission point of secondary protons along the x-axis. The beam entrance and exit faces of the PMMA are at $x_{\mathrm{PMMA}} = 2$ cm and $x_{\mathrm{PMMA}} = -2$ cm, respectively.

beam. The PMMA is mounted on a single-axis movement stage allowing position scans along the x-axis to be performed with a 0.2 mm accuracy (figure 1). In the configuration with the centers of PMMA, drift chamber and LYSO crystals aligned along the z-axis, the PMMA position in the stage reference frame is taken as 0 and will be referred to as the reference configuration.

From each track reconstructed in the drift chamber and backward extrapolated to the beam axis we can measure the x- and y-coordinates of the estimated emission point of the charged secondary particle, named x_{PMMA} and y_{PMMA}. The expected position of the BP obtained with the FLUKA simulation (Fasso' *et al* 2003) is located at (11.0 ± 0.5) mm from the beam entrance face of the PMMA, this value is confirmed from the direct observation of the PMMA deterioration after data taking, visible as a light yellow band and shown in figure 12 of Agodi *et al* (2012b). With the setup in the reference configuration, the beam entrance face of the PMMA is at $x = 2$ cm and therefore the expected position of the BP in our coordinate system (section 2) is $x_{\mathrm{Bragg}}|^{\mathrm{Ref}} = (9.0 \pm 0.5)$ mm. Figure 6 shows the distribution of the reconstructed x_{PMMA}, compared to the expected distribution of the dose deposition in the PMMA, both obtained with the setup in the reference configuration. The mean of the Gaussian fit to the distribution is $\bar{x}_{\mathrm{PMMA}} = 17.1 \pm 0.2$ mm, and consequently the separation between the BP and the peak from secondary proton emission is $\Delta_{\mathrm{ProtonBragg}} = 8.1 \pm 0.5$ mm. Figure 7 shows the distribution of the reconstructed x_{PMMA} and y_{PMMA} for all identified protons (solid line), for protons with $E_{\mathrm{kin}} > 60$ MeV (hatched) and for protons with $E_{\mathrm{kin}} > 100$ MeV (gray). The beam entrance and exit faces of the PMMA are at $x_{\mathrm{PMMA}} = 2$ cm and $x_{\mathrm{PMMA}} = -2$ cm and $y_{\mathrm{PMMA}} = 1.6$ cm and $y_{\mathrm{PMMA}} = -2.4$ cm. The x_{PMMA} distribution is related to the range of the beam, while the y_{PMMA} to its transversal profile. Quite remarkably the shape of the distribution of the emission point is approximately the same for protons emitted with different kinetic energies, e.g. the resolution on x_{PMMA} does not depend critically on the E_{kin} variable.

The existence of a relationship between the expected BP position and the peak of the x_{PMMA} distribution, as a function of the PMMA position, in principle could allow us to follow the BP position using the x_{PMMA} measurements. To estimate the accuracy of this method, a

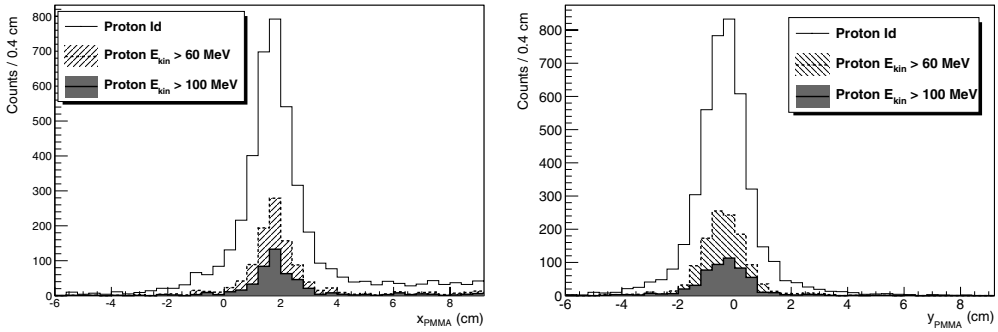

Figure 7. Distribution of x_{PMMA} (left) and y_{PMMA} (right) obtained for all charged particles identified as protons (black solid line), for protons with $E_{\mathrm{kin}} > 60$ MeV (dashed line) and with $E_{\mathrm{kin}} > 100$ MeV (gray). The beam entrance and exit faces of the PMMA are at $x_{\mathrm{PMMA}} = 2$ cm and $x_{\mathrm{PMMA}} = -2$ cm and $y_{\mathrm{PMMA}} = 1.6$ cm and $y_{\mathrm{PMMA}} = -2.4$ cm.

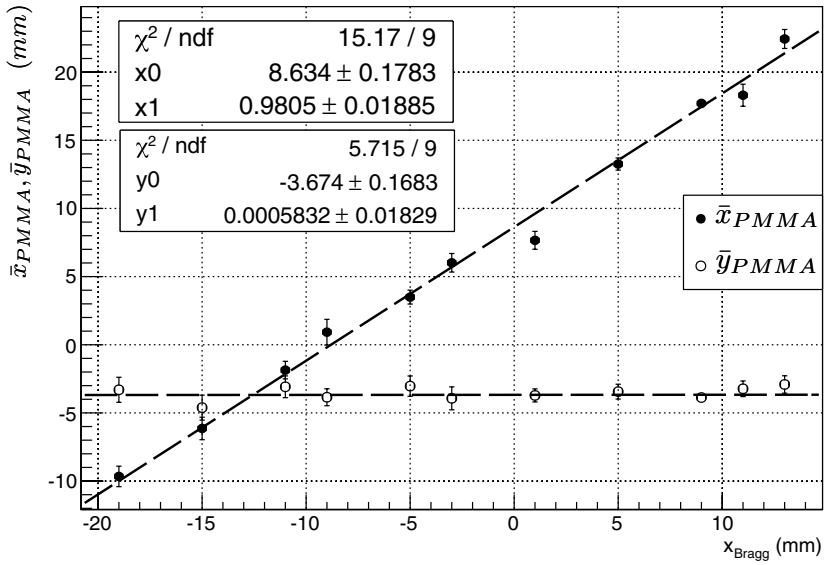

Figure 8. Reconstructed peak position of the secondary proton emission distribution $\bar{x}_{\mathrm{PMMA}}$, $\bar{y}_{\mathrm{PMMA}}$ as a function of the expected Bragg peak position x_{Bragg}, with $E_{\mathrm{kin}} > 60$ MeV.

position scan has been performed acquiring several data runs moving the PMMA by means of the translation stage.

For each run with different PMMA position, the production region of the protons has been monitored using the mean values of the Gaussian fit to x_{PMMA} and y_{PMMA} distributions, $\bar{x}_{\mathrm{PMMA}}$ and $\bar{y}_{\mathrm{PMMA}}$. Since $\bar{y}_{\mathrm{PMMA}}$ is the coordinate of the proton emission point along the vertical axis, and is related to the fixed beam profile in the transverse plane, its behavior as a function of the PMMA position provides an estimate of the method's systematic uncertainty.

Each PMMA position in the stage reference frame can be translated into the expected BP position x_{Bragg} for that given PMMA position. Figure 8 shows the results obtained for $\bar{x}_{\mathrm{PMMA}}$ and $\bar{y}_{\mathrm{PMMA}}$ as a function of x_{Bragg}, with $E_{\mathrm{kin}} > 60$ MeV protons. A clear linear relationship is

Table 1. Statistics of identified protons with $E_{\mathrm{kin}} > 60$ MeV, obtained with the position scan data.

x_{Bragg} (mm)	−19	−15	−11	−9	−5	−3	1	5	9	11	13
$N^{60\mathrm{MeV}}_{\mathrm{Protons}}$	67	77	88	61	92	75	113	154	1223	130	83

observed between $\bar{x}_{\mathrm{PMMA}}$ and x_{Bragg}, indicating that the charged secondary particles emission reconstructed with the drift chamber follows accurately the BP movement. No dependence of the $\bar{y}_{\mathrm{PMMA}}$ values on the BP position is observed, as expected from a translation of the PMMA along the x-axis only. Similar results can be obtained using protons with different E_{kin} selection, as it can be inferred from figure 7.

We evaluated the difference $\Delta_{\mathrm{ProtonBragg}} = \bar{x}_{\mathrm{PMMA}} - x_{\mathrm{Bragg}}$ for all identified protons and for the proton sample with $E_{\mathrm{kin}} > 60$ MeV. The $\Delta_{\mathrm{ProtonBragg}}$ root mean square is $\sigma_{\Delta_{\mathrm{ProtonBragg}}} \simeq 0.9$ mm for both samples. This can be explained as follows: in the sample with all identified protons, the contribution to the total uncertainty due to the scattering is partially compensated by the larger statistics with respect to the sample with $E_{\mathrm{kin}} > 60$ MeV. Table 1 reports the number of identified protons with $E_{\mathrm{kin}} > 60$ MeV obtained with the position scan data.

To evaluate the accuracy that might be achievable in the BP determination exploiting the proton signal, we have to evaluate the intrinsic fluctuation of the average emission point of the protons. To this aim several contributions need to be considered. The uncertainty $\sigma_{\mathrm{Extrapol}}$ due to the backward extrapolation of the track from the drift chamber to the beam line can be estimated from the root mean square of the $\bar{y}_{\mathrm{PMMA}}$ values, $\sigma_{\bar{y}_{\mathrm{PMMA}}} = \sigma_{\mathrm{Extrapol}} = 0.5$ mm. The latter contributes to the $\Delta_{\mathrm{ProtonBragg}}$ distribution, together with $\sigma_{\mathrm{Stage}} = 0.2$ mm from the uncertainty on the PMMA positioning. To be conservative, we can assume that all the other contributions to the total accuracy $\sigma_{\mathrm{ProtonBragg}}$, besides the quoted $\sigma_{\mathrm{Extrapol}}$ and σ_{Stage}, come from the shape of the distribution of the emission point of charged secondary particles $\sigma_{\Delta_{\mathrm{Emission}}}$. Consequently the total accuracy can be written as

$$\sigma_{\mathrm{ProtonBragg}} = \sqrt{\sigma^2_{\Delta_{\mathrm{Emission}}} + \sigma^2_{\mathrm{Extrapol}} + \sigma^2_{\mathrm{Stage}}}. \tag{1}$$

Using the quoted value for the estimated accuracies, we obtain $\sigma_{\Delta_{\mathrm{Emission}}} \sim 0.7$ mm. It must be stressed that this value represents only an indication of the precision achievable in the BP determination using secondary protons, due to the target thickness, atomic composition, density and homogeneity in the present setup, with respect to a possible clinical application.

5. Flux of charged secondary particles

The flux of the secondary protons emitted from the beam interaction with the PMMA has been measured at 90 ° with respect to the beam direction and in the geometrical acceptance of the triggering LYSO crystals, configuration maximizing the sensitivity to the BP position. The surface of the LYSO is 3×3 cm^2, corresponding to a solid angle $\Omega_{\mathrm{LYSO}} = 1.3 \times 10^{-4}$ sr at a distance of 74 cm. The proton's kinetic energy spectrum measured with data has been inserted in the FLUKA simulation to evaluate the detection efficiency in the LYSO crystals for protons with $E_{\mathrm{LYSO}} > 1$ MeV: $\epsilon_{\mathrm{LYSO}} = (98.5 \pm 1.5)\%$, with the uncertainty mainly due to the Monte Carlo statistics. To properly evaluate the rate of charged secondary particles reaching the LYSO crystals, the number of carbon ions reaching the PMMA target (N_{C}) has been computed according to Agodi *et al* (2012a): counting the number of signals in the start counter (N_{SC}) within randomly triggered time windows of $T_w = 2$ μs, corrected for the start counter efficiency $\epsilon_{\mathrm{SC}} = (96 \pm 1)\%$, and the acquisition dead time. The number of emitted secondary protons N_{P} has been measured with the x_{PMMA} distribution counts, corrected for ϵ_{SC},

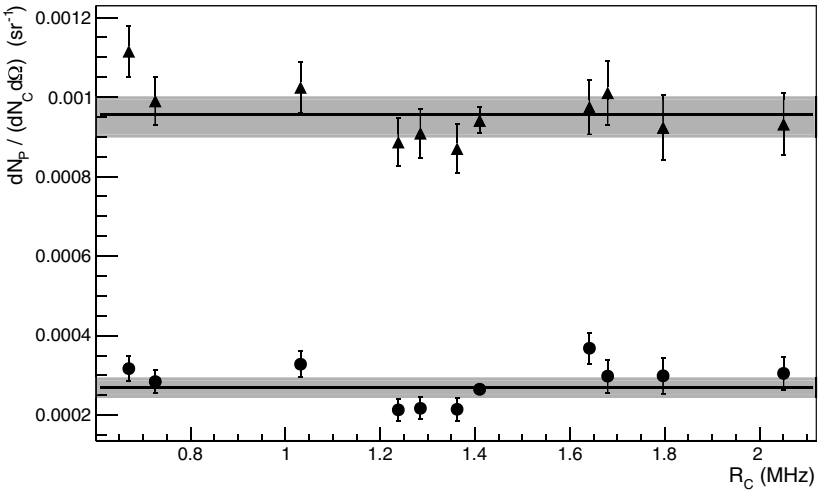

Figure 9. Double-differential production rate for secondary particles emitted at 90° with respect to the beam line, as a function of the rate of the carbon ions R_C reaching the PMMA target: all identified protons (triangles) and protons with $E_{kin} > 60$ MeV (circles).

ϵ_{LYSO}, the tracking efficiency $\epsilon_{Track} = (98 \pm 1)\%$ (Abou-Haidar *et al* 2012) and the acquisition dead time.

The double-differential production rate of secondary protons emitted at 90° with respect to the beam line is estimated as

$$\frac{d^2N_P}{dN_C\, d\Omega}(\theta = 90^\circ) = \frac{N_P}{N_C \Omega_{LYSO}}. \tag{2}$$

Figure 9 shows the double-differential production rate of secondary protons, emitted at 90° with respect to the beam line, as a function of the rate of the carbon ions R_C reaching the PMMA: all identified protons and protons with $E_{kin} > 60$ MeV. The fit result to the experimental points with a one-sigma uncertainty band is also shown. Expressing these results in terms of the secondary proton's kinetic energy at emission E_{kin}^{Prod}, we obtain

$$\frac{dN_P}{dN_C\, d\Omega}\left(E_{kin}^{Prod} > 7\,\text{MeV}, \theta = 90^\circ\right) = (9.56 \pm 0.18_{stat} \pm 0.40_{sys}) \times 10^{-4}\text{sr}^{-1}, \tag{3}$$

$$\frac{dN_P}{dN_C\, d\Omega}\left(E_{kin}^{Prod} > 83\,\text{MeV}, \theta = 90^\circ\right) = (2.69 \pm 0.08_{stat} \pm 0.12_{sys}) \times 10^{-4}\text{sr}^{-1}, \tag{4}$$

with the systematic contribution mainly due to proton identification and the uncertainty on the production kinetic energy related to the beam's transversal profile uncertainty.

The same experimental setup described in section 2 has been used to measure the differential production rate for prompt photons, with energy $E_{LYSO} > 2$ MeV and emitted at 90° with respect to the beam line: $dN_\gamma/(dN_C\, d\Omega)(E_{LYSO} > 2\,\text{MeV}, \theta = 90^\circ) = (2.92 \pm 0.19) \times 10^{-4}$ sr^{-1} (Agodi *et al* 2012a).

6. Discussion and conclusions

We reported the study of secondary charged particles produced by the interaction of 80 MeV/u fully stripped carbon ion beam of INFN-LNS laboratory in Catania with a PMMA target.

Protons have been identified exploiting the energy and time of flight measured with a plastic scintillator together with LYSO crystals, and their direction has been reconstructed with a drift chamber. A detailed simulation of the setup based on the FLUKA package has been done to evaluate its acceptance and efficiency, and to optimize secondary particle's identification.

It has been shown that the backtracking of secondary protons allows their emission region in the target to be reconstructed. Moreover, the existence of a correlation between the reconstructed production region of secondary protons and the Bragg peak (BP) position has been observed, performing a position scan of the target. The achievable accuracy on the BP determination exploiting this procedure has been estimated to be in the submillimeter range, using the described setup and selecting secondary protons with kinetic energy at emission $E_{\mathrm{kin}}^{\mathrm{Prod}} > 83$ MeV.

The obtained accuracy on the position of the released dose should be regarded as an indication of the achievable accuracy for possible applications of this technique to monitor the BP position in hadrontherapy treatment. In fact in clinical application, the secondary particles should cross a larger amount of material (patient tissue) resulting in an increased multiple scattering contribution worsening the BP resolution by, at most, a factor 2–3. On the other hand, an optimized device allowing a closer positioning to the patient could greatly improve the collected statistics of protons produced with $E_{\mathrm{kin}}^{\mathrm{Prod}} > 80$ MeV, reducing multiple scattering effects. Furthermore, the intrinsic good tracking resolution and high detection efficiency easily achievable in charged particle detectors, make this monitoring option worthwhile for further investigations.

The measured differential production rate for protons with $E_{\mathrm{kin}}^{\mathrm{Prod}} > 83$ MeV and emitted at 90° with respect to the beam line is $\mathrm{d}N_{\mathrm{P}}/(\mathrm{d}N_{\mathrm{C}}\mathrm{d}\Omega)\left(E_{\mathrm{kin}}^{\mathrm{Prod}} > 83\,\mathrm{MeV}, \theta = 90^{\circ}\right) = (2.69 \pm 0.08_{\mathrm{stat}} \pm 0.12_{\mathrm{sys}}) \times 10^{-4}\mathrm{sr}^{-1}$.

Acknowledgments

We would like to thank the precious cooperation of the staff of the INFN-LNS (Catania, Italy) accelerator group. The authors would like to thank Dr M Pillon and Dr M Angelone (ENEA-Frascati, Italy) for allowing us to validate the response of our detector to neutrons on the Frascati Neutron Generator; C Piscitelli (INFN-Roma, Italy) for the realization of the mechanical support; M Anelli (INFN-LNF, Frascati) for the drift chamber construction. This work has been supported by the 'Museo storico della fisica e Centro di studi e ricerche Enrico Fermi'.

References

Abou-Haidar Z *et al* 2012 Performance of upstream interaction region detectors for the FIRST experiment at GSI *J. Instrum.* **7** P02006

Agodi C *et al* 2012a Precise measurement of prompt photon emission from 80 MeV/u carbon ion beam irradiation *J. Instrum.* **7** P03001

Agodi C *et al* 2012b Study of the time and space distribution of β^+ emitters from 80 MeV/u carbon ion beam irradiation on PMMA *Nucl. Instrum. Methods Phys. Res.* B **283** 1–8

Amaldi U and Kraft G 2005 Radiotherapy with beams of carbon ions *Rep. Prog. Phys.* **68** 1861–82

Attanasi F, Belcari N, Del Guerra A, Enghardt W, Moehrs S, Parodi K, Rosso V and Vecchio S 2009 Comparison of two dedicated 'in beam' PET systems via simultaneous imaging of $^{(12)}$C-induced β^+-activity *Phys. Med. Biol.* **54** N29–35

Brahme A 1986 Optimal use of light ions for hadrontherapy *NIRST Symp. on Radiation Life Science* pp 18–40

Durante M and Loeffler J S 2010 Charged particles in radiation oncology *Nature Rev. Clin. Oncol.* **7** 37–43

Enghardt W, Crespo P, Fiedler F, Hinz R, Parodi K, Pawelke J and Pönisch F 2004 Charged hadron tumour therapy monitoring by means of PET *Nucl. Instrum. Methods Phys. Res.* A **525** 284–8

Fasso' A *et al* 2003 The physics models of FLUKA: status and recent development arXiv: hep-th/0306267
Ferrari A, Fasso A, Sala P R and Ranft J 2005 *FLUKA: A Multi Particle Transport Code* (Genera: CERN) pp 1–406
Fiedler F, Priegnitz M, Jülich R, Pawelke J, Crespo P, Parodi K, Pönisch F and Enghardt W 2008 In-beam PET measurements of biological half-lives of 12C irradiation induced beta+-activity *Acta Oncol.* **47** 1077–86
Jäkel O, Karger C P and Debus J 2008 The future of heavy ion radiotherapy *Med. Phys.* **35** 5653–63
Koba A, Iwamoto H, Kiyohara K, Nagasaki T, Wakabayashi G, Uozumi Y and Matsufuji N 2011 Scintillation efficiency of inorganic scintillators for intermediate-energy charged particles *Prog. Nucl. Sci. Technol.* **1** 218–21
Min C H, Kim C H, Youn M Y and Kim J W 2006 Prompt gamma measurements for locating the dose falloff region in the proton therapy *Appl. Phys. Lett.* **89** 183517
Paans A and Schippers J 1993 Proton therapy in combination with PET as monitor: a feasibility study *IEEE Trans. Nucl. Sci.* **40** 1041–4
Parodi K, Enghardt W and Haberer T 2002 In-beam PET measurements of $\beta +$ radioactivity induced by proton beams *Phys. Med. Biol.* **47** 21–36
Pawelke J, Enghardt W, Haberer T, Hasch B, Hinz R, Kramer M, Lauckner E and Sobiella M 1997 In-beam PET imaging for the control of heavy-ion tumour therapy *IEEE Trans. Nucl. Sci.* **44** 1492–8
Schardt D and Elsässer T 2010 Heavy-ion tumor therapy: physical and radiobiological benefits *Rev. Mod. Phys.* **82** 383–425
Stichelbaut F and Jongen Y 2003 *39th Meeting Particle Therapy Cooperative Group (San Francisco) (unpublished)*
Testa E, Bajard M, Chevallier M, Dauvergne D, Le Foulher F, Freud N, Létang J M, Poizat J C, Ray C and Testa M 2008 Monitoring the Bragg peak location of 73 MeV/u carbon ions by means of prompt γ-ray measurements *Appl. Phys. Lett.* **93** 093506
Testa E, Bajard M, Chevallier M, Dauvergne D, Le Foulher F, Freud N, Létang J M, Poizat J C, Ray C and Testa M 2009 Dose profile monitoring with carbon ions by means of prompt-gamma measurements *Nucl. Instrum. Methods Phys. Res.* B **267** 993–6
Vecchio S *et al* 2009 A PET prototype for in-beam monitoring of proton therapy *IEEE Trans. Nucl. Sci.* **56** 51–6